ISIJ International, Vol. 59 (2019), No. 7, pp. 1344–1353

Effect of Pearlite Volume Fraction on Two-step Ductile to Brittle Transition in Ferrite + Pearlite Structure Steel Sheets

Hiroyuki KAWATA[1)]* and Osamu UMEZAWA[2)]

1) Steel Research Laboratories, Nippon Steel & Sumitomo Metal Corporation, 20-1 Shintomi, Futtsu, Chiba, 293-8511 Japan.
2) Faculty of Engineering, Yokohama National University, 79-5 Tokiwadai, Hodogaya-ku, Yokohama, Kanagawa, 240-8501 Japan.

(*Received on November 14, 2018; accepted on January 29, 2019; J-STAGE Advance published date: March 22, 2019*)

Multi structural steels exhibit high strength and good formability; however, their performance depends on the volume fraction of the secondary phase. In our previous study, ferrite + pearlite structural steel sheet showed the characteristic two-step ductile-to-brittle transition (DBT) with decreasing temperature, and the absorbed energy curve exhibited a distinct middle shelf. In this study, we evaluated the effect of pearlite volume fraction (V_P) on the DBT behavior by the Charpy impact test with sub-size specimens. For specimens without pearlite, the absorbed energy directly dropped from the upper shelf to the lower shelf with decreasing temperature. For samples with 2–3% pearlite, the absorbed energy corresponding to the transition temperature range was dispersed between the two shelves, and the transition behavior seemed to be the typical DBT behavior. When V_P was increased to 21%, the absorbed energy just above the transition-finish temperature became stable at a middle level between the two shelves; thus, the existence of a distinct middle shelf was confirmed. Although the transition-start temperature increased with increasing V_P, V_P did not affect the transition-finish temperature and the absorbed energy at the middle shelf. These results were analyzed with a simple model based on the Yoffee diagram.

KEY WORDS: ductile to brittle transition; dual phase steel sheet; Charpy impact test; middle shelf.

1. Introduction

High-strength multi-structural steels are widely used because of their high performance. Dual phase (DP) steel, a typical multi-structural steel, consists of a soft ferrite phase and a hard structure formed by martensite, bainite, or pearlite. Although DP steels exhibit high strength and good formability, it is necessary to provide a fracture resistance in industrial use. Their mechanical properties depend on the volume fraction of the hard phase.[1)] Thus, it is important to clarify the fracture mechanism and significance of the hard structure.

Toughness is an important fracture property. Several studies have been performed on the fracture behavior of DP steels. For instance, the influence of volume fraction of martensite on the impact absorbed energy has been evaluated.[2–6)] However, it is difficult to determine the effect of volume fraction because the character of martensite depends on its carbon content, which changes with the volume fraction. In addition, the component characteristics, such as morphology[7,8)] and local strength,[4,9)] affect the impact property. Nevertheless, the basic effect of volume fraction on the impact fracture mechanism of DP steel has not been clearly determined in these studies.

In our previous study,[10)] we had investigated the ductile-to-brittle transition (DBT) with decreasing temperature in ferrite + pearlite DP structural steel sheets using a Charpy impact test with sub-size specimens. The absorbed energy showed a two-step DBT behavior with decreasing temperature[11)] and the transition curve showed a clear "middle shelf" (MS) between the upper shelf (US) and lower shelf (LS). In the MS, the absorbed energy remained at the middle level, and the fracture surface (FS) was found to be a cleavage-like surface with a few dimples. The crystallographic orientation analysis performed on the electron backscatter diffraction patterns indicated that the microstructure immediately below the FS at the MS absorbed the plastic strain; thus, the fracture mode at the MS was determined to be quasi-cleavage fracture (QCF).[12–14)] In addition, the fracture modes at the US and the LS were determined to be microvoid coalescence fracture (MVCF)[13)] and cleavage fracture (CF) propagating along the $\{001\}_{bcc}$ planes, respectively. Notably, the fracture mode in the ferrite + pearlite steel sheet transitioned from MVCF to QCF, and from QCF to CF with decreasing temperature. This characteristic feature of DBT was probably caused by the existence of two different structures.[10)] Therefore, we believe that the volume fraction of the hard phase (in particular, presence or absence), will fundamentally change the DBT behavior.

In this study, we evaluated the DBT behavior of DP steel sheets containing ferrite (soft phase) and various amounts

* Corresponding author: E-mail: kawata.z84.hiroyuki@jp.nssmc.com
DOI: https://doi.org/10.2355/isijinternational.ISIJINT-2018-764

© 2019 ISIJ

of pearlite (hard phase). These sheets were used because their local property could be easily controlled by fixing the transition temperature and the volume fraction of pearlite could be easily varied by varying the bulk carbon content.

2. Experimental Procedure

2.1. Materials

Six kinds of steel sheets were prepared in the laboratory scale. **Table 1** lists the chemical compositions of the sheets. The carbon content ranged from 0.005 to 0.150 mass%; however, the P, S, Al, and N contents were low.

Table 1. Chemical compositions of test steel sheets (in mass%).

Steel	Content (mass%)						
	C	Si	Mn	P	S	Al	N
A	0.005	1.02	1.96	0.005	0.001	0.006	0.0008
B	0.016	1.02	1.99	0.005	0.001	0.006	0.0009
C	0.034	1.02	1.96	0.005	0.001	0.006	0.0009
D	0.065	1.00	1.95	0.004	0.001	0.007	0.0009
E	0.097	0.99	1.95	0.005	0.001	0.006	0.0009
F	0.150	0.98	1.95	0.005	0.001	0.006	0.0009

In addition, Si (1 mass%) and Mn (2 mass%) were added to strengthen the sheets. The ingots, after being melted in a vacuum induction furnace, were hot-rolled at 1 173 K to attain a thickness of 3.5 mm; subsequently, the sheets were kept at 923 K for 1 h and air cooled to room temperature. Later, the steel sheets were again annealed at 923 K for 3 h.

Figure 1 shows the scanning electron microscopy (SEM) images of the fabricated steel sheets, observed at half thickness along the transverse direction. The white patches seen in the images are pearlite islands. As observed, steel A (Fig. 1(a)) contains some polygonal ferrite grains without any pearlite. In other sheets, some pearlite (P) islands are observed among the ferrite grains. **Table 2** lists the average ferrite grain diameter (d_α) and the pearlite volume fraction (V_P) of the prepared sheets, evaluated by a point counting method. As observed, V_P increases with increasing carbon content. **Figure 2**(a) shows the phase diagram of Fe–1 mass% Si–2 mass% Mn–C system, obtained using Thermo–Calc with the TCFE8 material database. As seen in this diagram, the eutectoid point lies at 0.674 mass% C, and the maximum amount of solute carbon in ferrite is 0.005 mass% (932 K). Figure 2(b) shows the relationship between V_P and the carbon content. The eutectoid point (0.674 mass% C, full-pearlite structure) can be connected to the point corresponding to the maximum solute carbon content (0.005

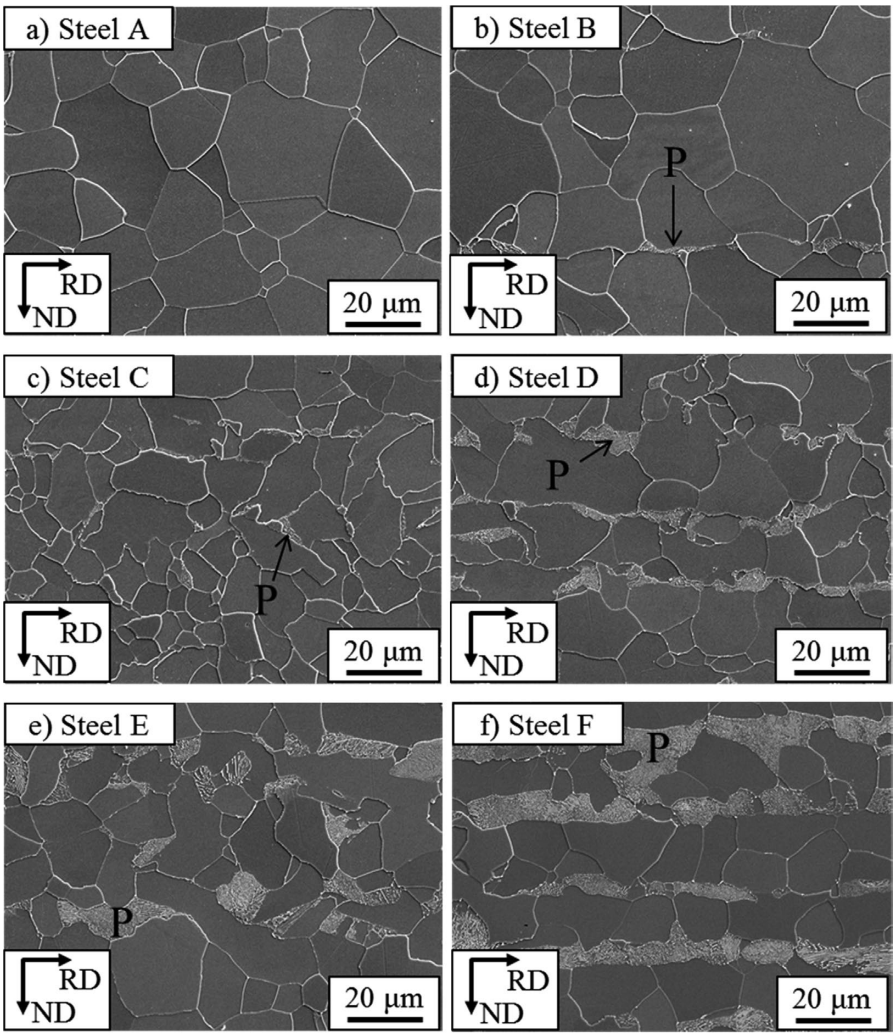

Fig. 1. SEM images of ferrite + pearlite steel sheets observed along the transverse direction (P indicates pearlite island).

© 2019 ISIJ

Table 2. Average ferrite grain diameters (d_α) and pearlite volume fractions (V_P) of steel sheets used.

Steel	d_α/(μm)	V_P (%)
A	18	0
B	15	2
C	11	3
D	13	7
E	11	16
F	11	21

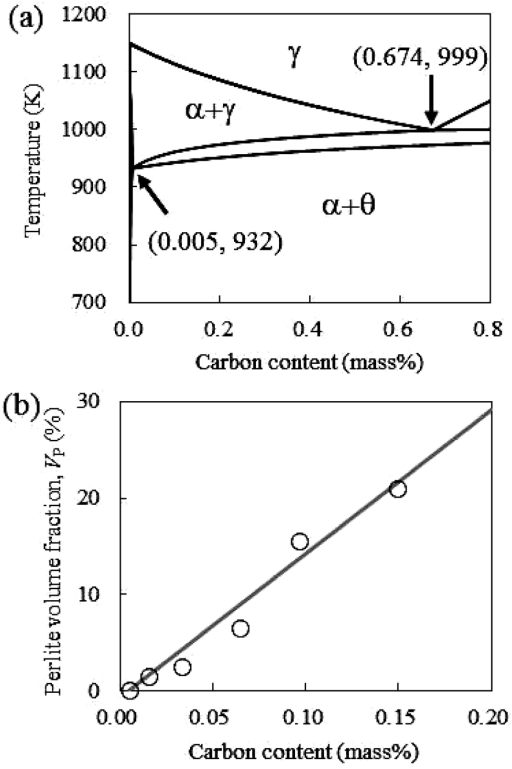

Fig. 2. (a) Calculated phase diagram for Fe–1mass%Si–2mass%Mn–C system. (b) Relationship between carbon content and pearlite volume fraction in steel sheets used. The bold line corresponds to the estimated volume fraction based on the phase diagram.

mass% C, full- ferrite structure) with a solid line. The results indicate that carbon content in the pearlite region of each sheet corresponds to that at the eutectoid point.

Table 3 lists the tensile properties of the sheets, evaluated with a 10-mm strain gage. As observed, with increasing carbon content, 0.2% proof stress and the maximum tensile strength increase, but the elongation decreases. Notably, these properties depend on V_P and d_α (Table 2).

2.2. Charpy Impact Test

DBT behaviors of the prepared sheets were evaluated by the Charpy impact test with sub-size specimens[10] in the temperature range from 77 K to room temperature (~297 K). The fabricated steel sheets were ground to 2.0 mm thickness on both surfaces to remove the decarbonized layer. The sub-size specimens made from these sheets were 55 mm in length (parallel to the transverse direction) and

Table 3. Tensile properties of steel sheets used. $\sigma_{0.2\%}$: 0.2% proof stress, TS: maximum tensile stress, and El: total elongation.

Steel	$\sigma_{0.2\%}$ (MPa)	TS (MPa)	El (%)
A	330	428	42
B	345	442	40
C	350	462	40
D	359	490	38
E	365	521	36
F	374	553	32

10 mm in width (along the rolling direction). For the test, a 2 mm V-notch was cut into the center of each specimen. The fracture propagated perpendicularly to the transverse direction along the rolling direction. The input energy of the test was 300 J. The specimens were immersed in denatured alcohol, then maintained in the temperature range 173–263 K. For temperatures below 153 K, the specimens were first immersed in liquid nitrogen. After being sufficiently cooled, the specimens were taken out. Later, when the specimen temperature reached the target temperature, the tests were performed.

After the impact tests, we characterized FSs of some samples using field-emission SEM (FE-SEM, JEOL–6500F). From the SEM images, we evaluated the area fraction of the low-energy fracture surface (LEFS)[10] with respect to the whole FS. The LEFS was flat (macroscopic view), with very few dimples (microscopic view). The LEFS included the cleavage fracture surface (CFS) and the quasi-cleavage fracture surface (QCFS).

3. Results

3.1. DBT in Ferritic Steel

Figure 3 shows the temperature-dependent absorbed energy behavior of the fully ferritic steel sheet A, indicating a DBT. As seen in Fig. 3(a), the absorbed energy separates into two levels: the US and the LS. The US exists at ~1 700 kJ/m^2 in the temperature range 143–297 K. On the other hand, the LS exists at ~100 kJ/m^2 in the temperature range 77–163 K. Thus, the DBT region corresponds to the temperature range from 143 K to 163 K. Although 23 samples were tested in this region, there was only one sample with absorbed energy in the middle range between the US and the LS.

The FS analysis of specimens showed similar results. Figure 3(b) shows the LEFS fraction corresponding to the absorbed energy shown in Fig. 3(a). The absorbed energy was normalized using the average US absorbed energy (1 772 kJ/m^2) in the temperature range 173–297 K which was over the DBT region. The FSs of LS specimens are LEFSs (without any dimples), and those of US specimens are MVCF surfaces, which were covered by dimples.

Figure 4 presents the fractographs of the fracture surfaces at half thickness, 500 μm away from the tip of notch, belonging to sheet A samples corresponding to the LS. The FSs of specimens failed at 133 K and 153 K during transition are shown in Figs. 4(a) and 4(b), respectively.

© 2019 ISIJ

As observed, both the surfaces are similar and without any dimples, typical of LS cleavage FSs. This result suggests that the DBT in steel sheet A the direct transition from MVCF to CF.

3.2. DBT in Ferrite + Pearlite Structure (V_p < 5%)

Figure 5 shows the absorbed energy change with decreasing temperature in steel sheets B and C containing small amounts of pearlite, 2 and 3%, respectively. For steel sheet B (Fig. 5(a)), the absorbed energy clearly exhibits both US and LS. The US exists between 297 K and 143 K at ~1 700 kJ/m^2, and the LS exists between 163 K and 77 K at ~80 kJ/m^2. As can be seen, this result is similar to that of steel A (Fig. 3(a)). However, several samples of steel sheet B tested between 183 K and 143 K showed absorbed energies dispersed between the US and the LS. Out of 25 specimens tested between 183 and 143 K, 13 of them did not exhibit distinct US nor LS. Thus, this temperature range was recognized as the DBT region of steel sheet B; steel B specimens could be separated into three groups depending on the absorbed energies.

Figure 5(b) shows the absorbed energy change in steel sheet C containing 3% pearlite. The US exists between 296 and 163 K at ~1 700 kJ/m^2, and the LS exists between 143 and 77 K at ~100 kJ/m^2. Notably, 10 specimens, out of 19, which were tested between 173 and 143 K, exhibited absorbed energies between the US and the LS. Further, the US temperature range did not overlap with that of the LS; thus, the absorbed energy distribution in Fig. 5(b) looks like

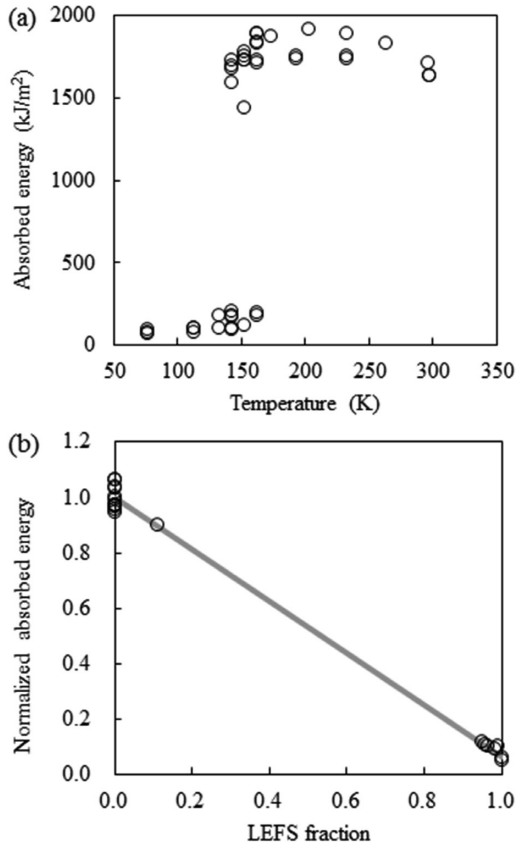

Fig. 3. (a) Absorbed energy transition behavior with temperature in fully ferritic steel sheet A. (b) Relationship between low-energy fracture surface (LEFS) fraction of the whole fracture surface and normalized absorbed energy (absorbed energy of each specimen divided by average absorbed energy at upper shelf). Bold line in (b) connects upper shelf and lower shelf.

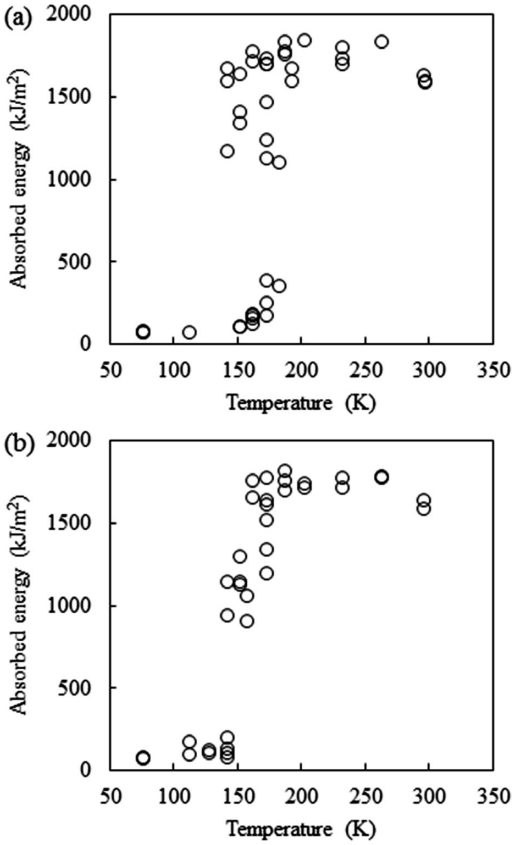

Fig. 5. Absorbed energy transition behaviors of (a) steel sheet B containing 2% pearlite and (b) steel sheet C containing 3% pearlite.

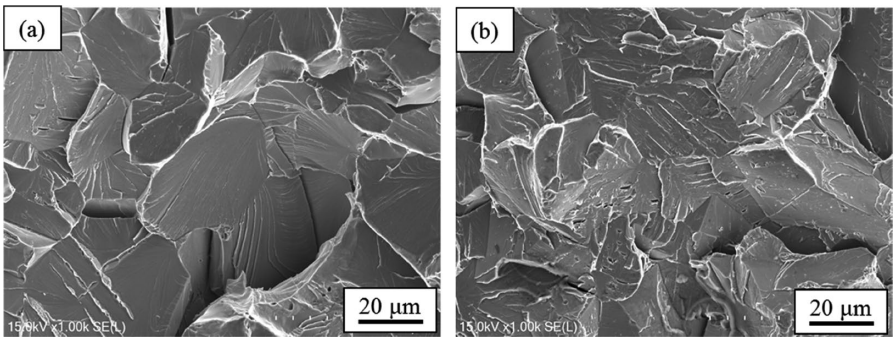

Fig. 4. Magnified images of fracture surface at 1/2 thickness of fully ferritic steel sheet A: (a) failed at 133 K and (b) failed at 153 K.

© 2019 ISIJ

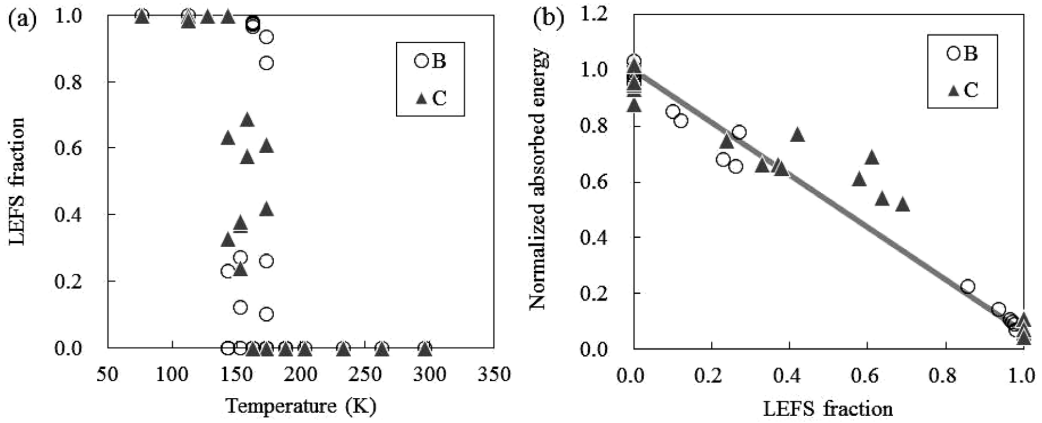

Fig. 6. (a) Fracture surface transition with temperature in ferrite + pearlite steel sheets B and C. (b) Relationship between low-energy fracture surface (LEFS) fraction of the whole fracture surface and normalized absorbed energy (absorbed energy of each specimen divided by average absorbed energy at upper shelf) in steel sheets B and C. Bold line connects upper shelf and lower shelf in steel sheet C.

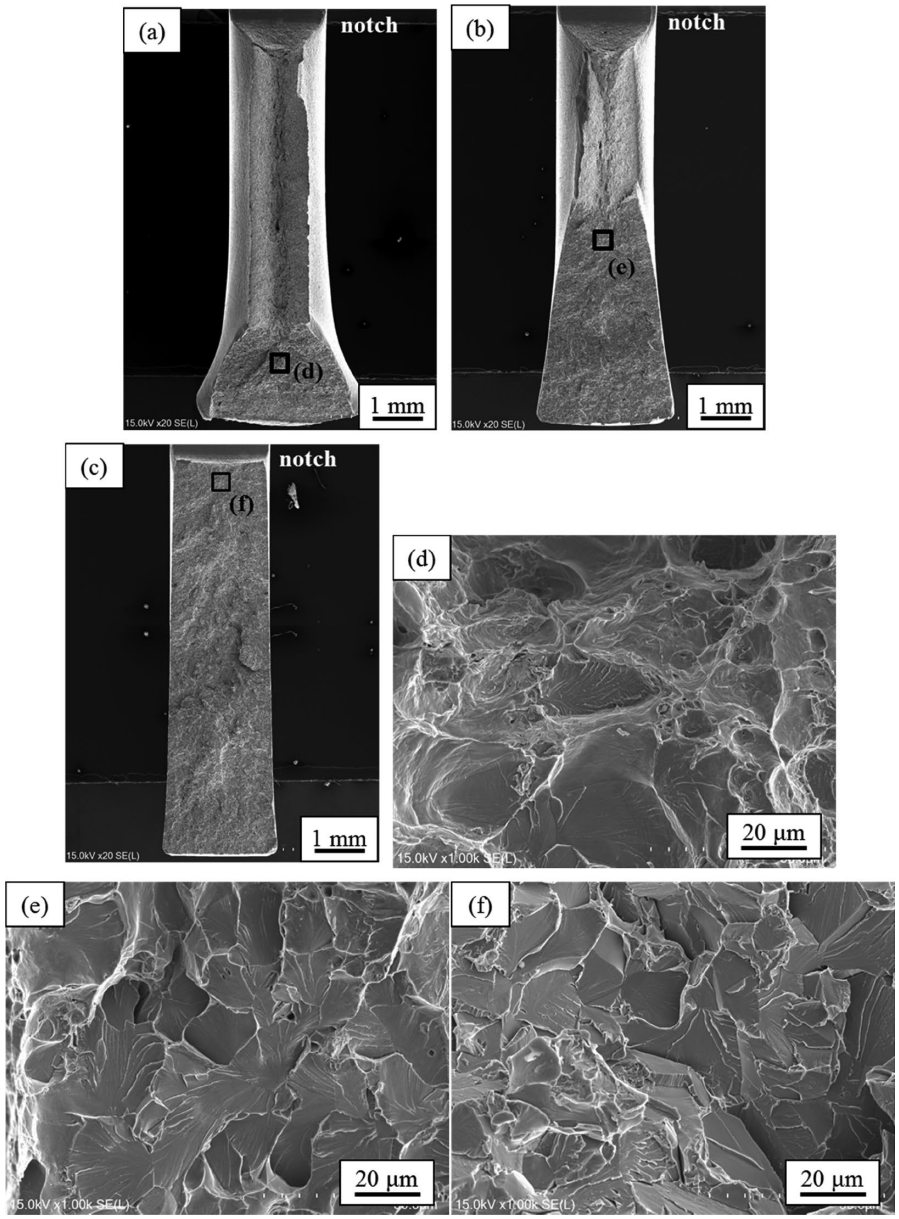

Fig. 7. Fracture appearance of sub-size Charpy impact specimens of steel sheet C tested at (a, d) 153, (b, e) 143, and (c, f) 128 K. (d), (e), and (f) are magnified images of areas marked with square boxes in macroscopic images (a), (b) and (c), respectively.

© 2019 ISIJ

the DBT "curve." The transition-start temperature is in the range 183–173 K, and the transition-finish temperature is in the range 143–128 K.

Figure 6(a) shows the LEFS fraction change with temperature in steel sheets B and C. As observed, in the transition region, the FS is partially LEFS. Figure 6(b) shows the relationship between the LEFS fraction and the absorbed energy that was normalized using the average US absorbed energy, in the transition region. The average US absorbed energies in the temperature range 183–297 K were 1 716 and 1 724 kJ/m^2 in steel sheets B and C respectively. The bold line in Fig. 6(b) links US, where the normalized absorbed energy is 1.00 and the FS is zero-LEFS, to LS, where the normalized absorbed energy is 0.06 (=100 (kJ/m^2)/1 724 (kJ/m^2.)) and the FS is wholly LEFS. This line corresponds to steel sheet C, and the line for steel sheet B overlapping this line is omitted in Fig. 6(b). This line represents the expected value, which based on the simple mixture of the fracture modes at the US and the LS. Most steel sheet B specimens show an intermediate absorbed energy, corresponding to their FS character. On the other hand, for steel sheet C, the absorbed energy in the transition region is higher than the expected value.

Figure 7 shows the fractographs of steel sheet C samples. Figures 7(a), 7(b), and 7(c) are macroscopic images of the specimens failed at 153, 143, and 128 K, respectively. The respective absorbed energies of these specimens are 1 294, 938, and 106 kJ/m^2, and the LEFS fractions are 24, 64, and 100%. This shows that the absorbed energy decreases with increasing LEFS fraction. Figures 7(d), 7(e), and 7(f) are magnified images of the LEFSs shown in Figs. 7(a), 7(b), and 7(c). For the sample failed at the LS, there is no sign of heavy plastic deformation and ductile fracture on the FS (shown in (f)). On the other hand, for specimens failed at the transition region, the LEFSs shown in (d) and (e) are cleavage-like FSs containing some dimples and tear-ridges, which are the characteristics of a ductile fracture. This result indicates that the LEFSs transitioned transformed from QCFS to CFS with decreasing temperature, in the transition region to the LS.

3.3. DBT in Ferrite + Pearlite Structure (V_p > 5%)

Figure 8 shows the absorbed energy transition behavior with decreasing temperature in steel sheets D, E and F containing 7, 16, and 21% pearlite, respectively. For steel sheet D samples (Fig. 8(a)), the absorbed energy curve is a typical transition curve, with distinct US and LS. As seen, DBT occurs between 203 K and 143 K. Notably, 24 samples were tested at 188 K and 153 K, and the absorbed energies of these samples were found to be at the medium level. As observed in Fig. 8(a), at 173, 163, and 143 K, the absorbed energy distribution is wide. In contrast, the distribution of the absorbed energy at 153 K is narrow.

Figures 8(b) and 8(c) show the absorbed energy plots of steel sheets E and F. As seen, the transition curves are similar. These curves show distinct US and LS. The transition starts between 263 K and 233 K, and finishes at just below 143 K for these samples. The absorbed energy distributions of steel sheets E and F are wide at 143 K, similar to that of steel sheet D (Fig. 8(a)). However, the absorbed energy looks stable (500 kJ/m^2) at 173 K. **Figure 9** shows the macroscopic fractographs of steel sheet F samples. The LEFS fraction increases with decreasing temperature, and the FS failed at 173 K (Fig. 9(d)), resulting in 94% LEFS. The fractographs shown in Figs. 9(a)–9(d) indicate typical DBT behavior: the absorbed energy decreases with increasing LEFS fraction, from 233 K to 173 K. However, the fractographs in Figs. 9(d)–9(g) suggest the occurrence of another transition at ~143 K. This two-step DBT, from US to LS, is similar to that observed in our previous study.[10] Figure 9(h) shows the magnified fractograph of the sample failed at 173 K (see Fig. 9(d)). The FS containing some dimples is determined to be a QCFS.

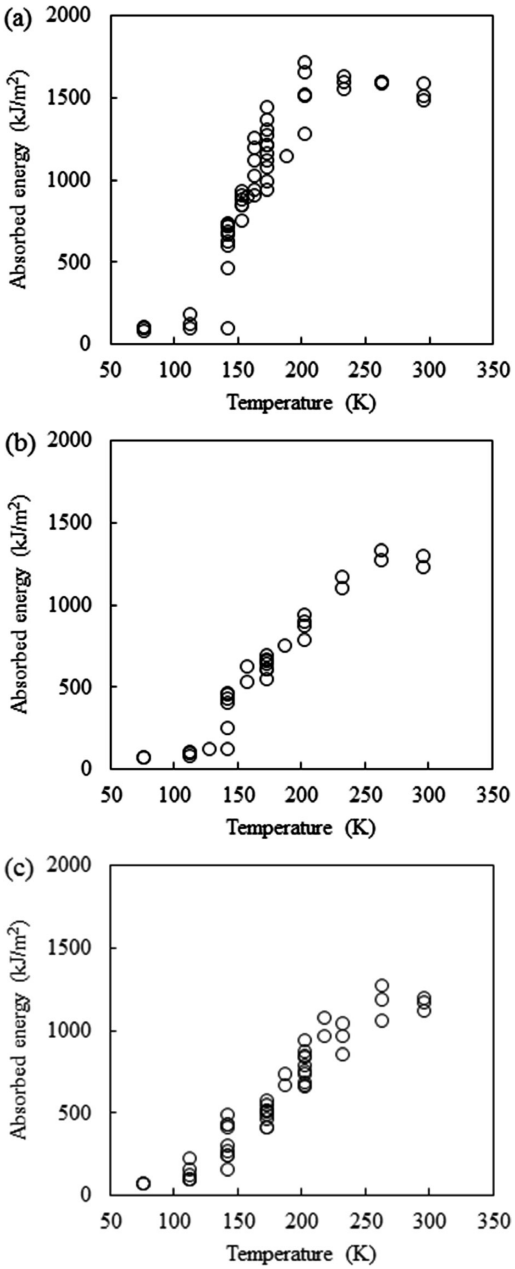

Fig. 8. Absorbed energy transition behaviors in (a) steel sheet D containing 7% pearlite, (b) steel sheet E containing 16% pearlite, and (c) steel sheet F containing 21% pearlite.

Figure 10 shows the relationship between absorbed energy and LEFS fraction for steel sheets D, E, and F into the transition region, similar to that shown in Fig. 6(b). The average US absorbed energies in the temperature ranges above the DBT regions were 1 567, 1 278, and 1 164 kJ/m^2,

© 2019 ISIJ

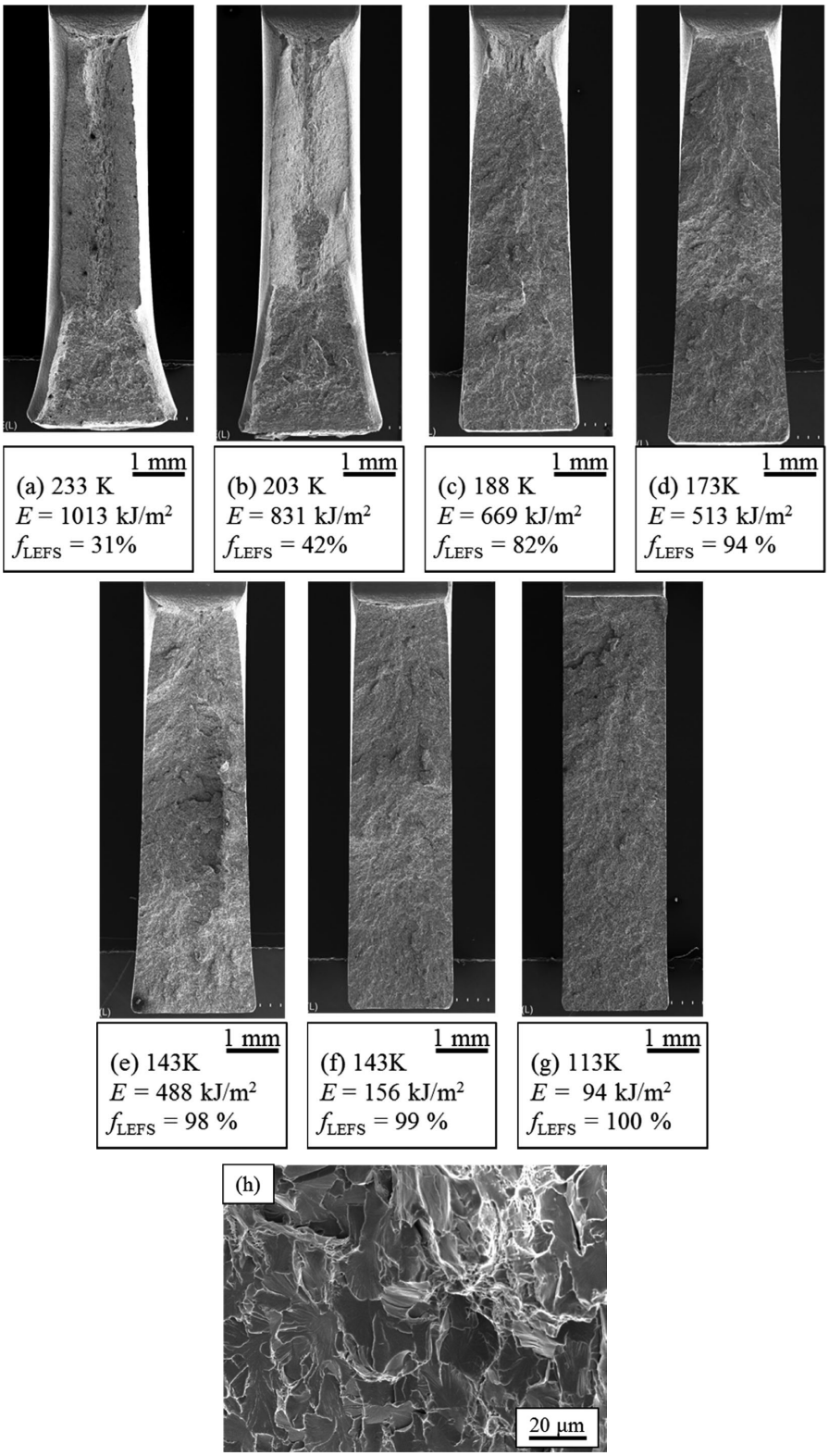

Fig. 9. Fracture appearance of sub-size Charpy impact specimens of steel sheet F tested from (a) 233 K to (g) 113 K, and (h) is magnified image corresponding to (d) the sample failed at 173 K. E: the absorbed energy, and f_{LEFS}: fraction of low-energy fracture surface.

respectively. The bold line in Fig. 10 links US to LS, where the normalized absorbed energy is 0.09 (=108 (kJ/m^2)/1 164 (kJ/m^2.)) and the FS is wholly LEFS. This line corresponds to steel sheet F, and the lines for steel sheets D and E overlapping this line are omitted in Fig. 10. As seen, the absorbed energy decreases with increasing LEFS fraction in a proportional manner. However, the absorbed energy is higher than the expected value, which depends on the absorbed energies at US and LS. We call this transition the "first transition.[10]" Moreover, around 100% LEFS fraction, the absorbed energy continues to decrease with slight change in the LEFS fraction, as seen in Fig. 10. This decrease corresponds to the absorbed energy transition in specimens that failed at 143 K, whose FSs are almost wholly

© 2019 ISIJ

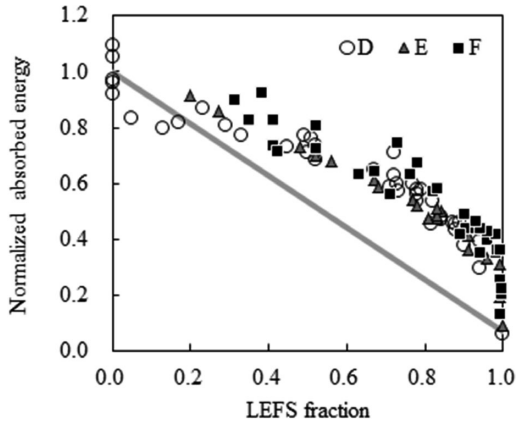

Fig. 10. Relationship between low-energy fracture surface (LEFS) fraction with respect to the whole fracture surface and normalized absorbed energy (absorbed energy of each specimen divided by average absorbed energy at upper shelf) in steel sheets D, E, and F. Bold line connects upper shelf and lower shelf in steel sheet F.

LEFS. We call this transition the "second transition.[10]" Thus, the DBT in steel sheets D, E, and F consisted of two steps (the first transition and the second transition) in which the relationship between the LEFS fraction and the absorbed energy was different from each other.

3.4. Effect of V_P on DBT Behavior

Figure 11 shows the effect of V_P on DBT in steel sheets prepared in this study. As seen in Fig. 11(a), the transition-start temperature increases, and finally, saturates with increasing V_P. However, the transition-finish temperature does not change with V_P; therefore, the transition region in between these temperatures widens with increasing V_P. In addition, the absorbed energy at the US (Fig. 11(b)) decreases with increasing V_P, and that at the LS remains constant. These results agree with those of a previous study performed by Burns with full-size Charpy specimens.[15]

The two-step DBT involves a MS. The specimens, which were failed just above the transition-finish temperature (143 K) in steel sheets D, E, and F, show the relatively stable absorbed energies with the FSs almost covered by LEFS, as shown in Figs. 8 and 9(d). We evaluated the absorbed energy at the MS in steel sheets D, E, and F from the plot in Fig. 10. Because the FS at MS is wholly LEFS, its absorbed energy is expected to be higher than or equal to a value corresponding to the intersection point of the line representing the first transition and the right axis in Fig. 10. Figure 11(b) shows the absorbed energy at the MS evaluated on the basis of lines approximating the data from the first-transition region. As seen, the absorbed energy at the MS in steel sheets D, E, and F are similar and independent of V_P.

4. Discussion

Figure 12 presents the schematics of DBT behaviors of ferritic steel sheets containing various amounts of pearlite. The three groups of schematics show the absorbed energy transition behavior with decreasing temperature (Figs. 12(a)–12(c)), FS transition behavior with decreasing temperature (Figs. 12(d)–12(f)), and relationship between absorbed energy and LEFS fraction (Figs. 12(g)–12(i)).

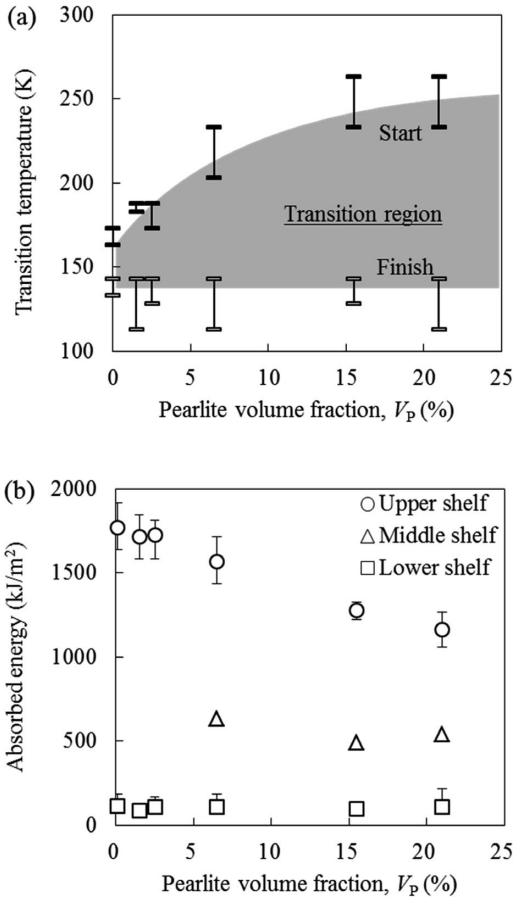

Fig. 11. Effect of pearlite volume fraction on (a) transition-start and transition-finish temperatures and (b) absorbed energies at upper, middle, and lower shelves.

For a fully ferritic steel sheet, such as steel sheet A (Fig. 3), the DBT behavior is described by Figs. 12(a), 12(d), and 12(g). With decreasing temperature, the absorbed energy directly drops from the US to the LS. Further, in the transition region, the absorbed energies of specimens are either US or LS; none of the specimens exhibited medium-level absorbed energy.

For a ferrite + pearlite steel sheet containing a very small amount of pearlite, such as steel sheets B and C (Figs. 5 and 6), the DBT behavior is described by Figs. 12(b), 12(e), and 12(h). The LEFS fraction ranges between 0% and 100% in the transition region. In addition, the absorbed energy decreases with decreasing temperature, but is linearly proportional to the LEFS fraction change. This behavior is usual DBT in common low carbon steels.

In a ferrite + pearlite steel sheet containing a large amount of pearlite, such as steel sheets E and F (Figs. 8–10), the DBT behavior is described by Figs. 12(c), 12(f), and 12(i). The transition involves two steps. During the first transition, the absorbed energy decreases from the US to the MS with decreasing temperature. At the MS, the absorbed energy stays at the middle level, and the FS is wholly LEFS. With further decrease in temperature, absorbed energy decreases from the MS to the LS. During the first transition, although the fracture mode changes from QCF to CF, the macroscopic features and the LEFS fraction almost remain constant. This two-step DBT behavior clearly corresponds to the relationship between absorbed energy and LEFS frac-

© 2019 ISIJ

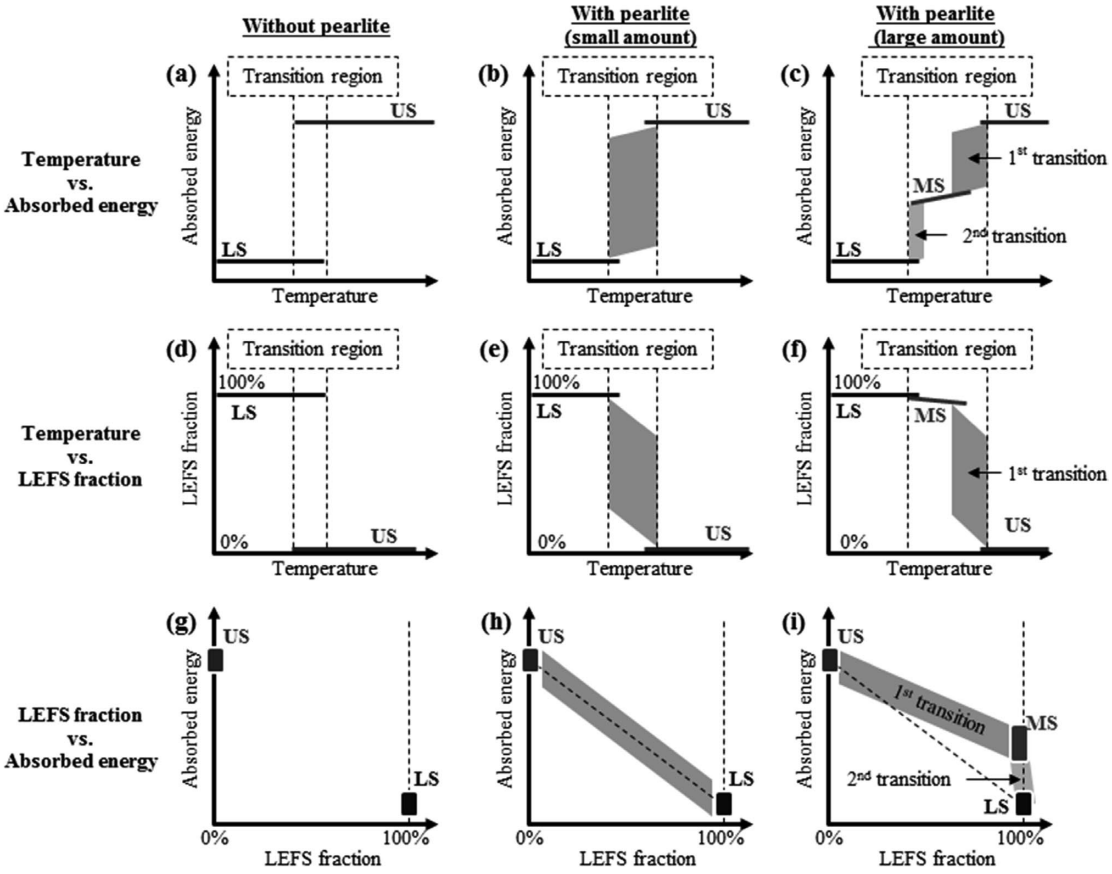

Fig. 12. Schematics of ductile to brittle transition in ferrite + pearlite structural steel sheets containing various amounts of pearlite (zero, small, and large).

tion, as shown in Fig. 12(i). In this study, steel sheets E and F with V_P 16 and 21%, respectively, showed this behavior. Such a behavior was not clearly observed in steel sheet D containing 7% pearlite.

In our previous study,[10] we had proposed a simple model based on "Yoffee diagram"[16] for two-step DBT behavior. **Figure 13**(a) shows the schematic of the proposed model. This model suggests that the first transition occurs when the yield stress of pearlite ($\sigma_{Y,P}$) becomes larger than the brittle fracture stress of pearlite ($\sigma_{F,P}$) with decreasing temperature. In this case, brittle fracture occurs in pearlite after plastic deformation in ferrite. Similarly, the second transition occurs when the yield stress of ferrite ($\sigma_{Y,\alpha}$) becomes larger than $\sigma_{F,P}$. However, in this case, brittle fracture can occur in pearlite without plastic deformation. Notably, the fracture mode shifts from MVCF to QCF, and from QCF to CF during these transitions.

Figures 13(b), 13(c), and 13(d) show the schematics of the model proposed in this study, which is based on the previous model, to explain the effect of V_P. The fully ferritic structure (Fig. 13(b)) exhibits one yield stress and one fracture stress. At high temperatures, $\sigma_{Y,\alpha}$ is smaller than the brittle fracture stress of ferrite ($\sigma_{F,\alpha}$); thus, the ferrite deforms plastically and fails, as per the MVCF mode. At low temperatures, because $\sigma_{Y,\alpha}$ is larger than $\sigma_{F,\alpha}$, brittle fracture starts during elastic deformation. Therefore, the fracture mode directly changes from MVCF to CF, as shown in Figs. 12(a), 12(d), and 12(g). In each ferrite specimen, the transition corresponding to the intersection of the stresses occurs over a temperature range rather than at a particular

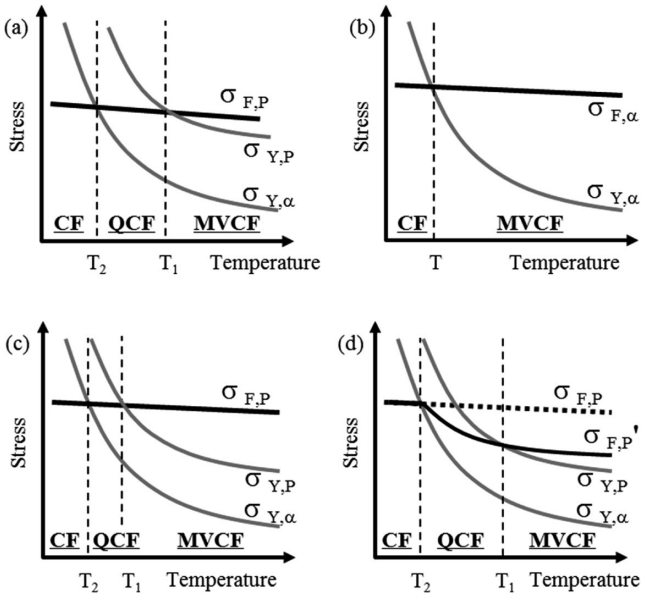

Fig. 13. Schematics showing relation among the yield stresses, fracture stress, and ductile to brittle transition (DBT) temperatures in ferrite + pearlite steel sheets. (a) our previous model for two-step DBT,[10] (b) model for fully ferritic steel sheet, (c) model for ferrite + a small amount of pearlite steel sheet, and (d) modified model for two-step DBT in ferrite + pearlite steel sheet. CF: cleavage fracture, QCF: quasi-cleavage fracture, MVCF: micro-void coalescence fracture, $\sigma_{Y,\alpha}$ and $\sigma_{Y,P}$: yield stresses of ferrite and pearlite, respectively, $\sigma_{F,P}$: brittle fracture stress of pearlite, and T_1, and T_2: typical, first and second transition temperatures, respectively.

© 2019 ISIJ

value because of the stresses variations.[17)]

In a specimen containing small amount of pearlite, the diagram, Fig. 13(c) is similar with our previous model, Fig. 13(a). However, because the difference between two transition temperatures is small, the fracture mode easily transits according to the stresses variations in the specimen. Thus, the actual transition occurs in a narrow temperature range, and the distribution of the absorbed energy is large, as shown in Fig. 12(b).

With the previous model (Fig. 13(a)), it is difficult to explain the effect of V_P, because it does not include the V_P-induced stress change. Therefore, we propose the modified diagram, as shown in Fig. 13(d). For a dual phase structure, strain and stress distributions in each phase change with the volume fraction during plastic deformation. Wang *et al.*[18)] estimated these distributions in a ferrite + pearlite structure on the basis of the iso-work assumption,[19)] and suggested that the applied strain and stress at the same total strain increase with V_P. On the basis of this prediction, it is presumed that $\sigma_{F,P}$ during plastic deformation ($\sigma_{F,P}$') becomes smaller than $\sigma_{F,P}$ (without plastic deformation, the dotted line) with increasing V_P (see Fig. 13(d)). This shift increases the first-transition temperature to a value corresponding to the intersection between $\sigma_{F,P}$' and $\sigma_{Y,P}$. On the contrary, it does not affect the second-transition temperature, because this temperature depends on the properties related to elastic deformation.

In between first and second transitions, the specimen undergoes plastic deformation before fracture. This deformation is reflected in the fractographs as macroscopic shape changes (Fig. 9), corresponding to the absorbed energy at the MS. It is one of the sources of the absorbed energy at the MS, which is larger than that absorbed at the LS. Fracture occurrence and propagation are the other sources. Notably, because the propagation path at the MS is different from that at the LS,[20)] the energy required for the fracture propagation at the MS is possibly larger than that at the LS.

5. Summary

In this study, we investigated the effect of secondary-phase volume fraction on the DBT of dual phase structure steel. For the study, we used ferrite + pearlite structural steel sheets containing 0–21% pearlite.

(1) In the fully ferritic structure (without pearlite), the absorbed energy directly dropped from the US to the LS with decreasing temperature. None of the specimens exhibited middle-level absorbed energy, between the US and the LS, and LEFS fractions corresponding to middle-level energy.

(2) Some specimens of the steel sheet containing 2% pearlite exhibited middle-level absorbed energy, between the US and the LS, and LEFS fractions corresponding to middle-level energy. Further, for specimens of the steel sheet containing 3% pearlite, the absorbed energy remained at the middle level. In addition, the LEFS fractions of the specimens that failed between the transition-start and transition-finish temperatures corresponded to middle-level energy; thus, their transition behaviors corresponded to typical transition "curves."

(3) In steel sheets containing 16% and 21% pearlite, the absorbed energy just above the transition-finish temperature was stable at the middle level (~500 kJ/m^2), and the FS was almost wholly LEFS. In addition, these sheets exhibited MS. Moreover, the DBT involved two steps.

(4) For steel sheets containing 7, 16, and 21% pearlite, the absorbed energy during transition was larger than that estimated from LEFS fraction plot.

(5) The transition-start temperature increased, and the absorbed energy at US decreased with increasing V_P. In contrast, the transition-finish temperature and the absorbed energy at MS and LS did not change with increasing V_P.

REFERENCES

1) N. Fonstein: Advanced High Strength Sheet Steels, Springer International Publishing, Switzerland, (2015), 67.
2) A. Bag, K. K. Ray and E. S. Dwarakadasa: *Metall. Mater. Trans. A*, **30** (1999), 1193.
3) A. Bag, K. K. Ray and E. S. Dwarakadasa: *Metall. Mater. Trans. A*, **32** (2001), 2207.
4) S. S. M. Tavares, P. D. Pedroza, J. R. Teodosio and T. Gurova: *Scr. Mater.*, **40** (1999), 887.
5) F. Hayat and H. Uzun: *J. Iron Steel Res. Int.*, **18** (2011), 65.
6) I. Pushkareva, S. Allain, C. Scott, A. Redjaimia and A. Moulin: *ISIJ Int.*, **55** (2015), 2237.
7) M. Calcagnotto, D. Ponge and D. Raabe: *Mater. Sci. Eng. A*, **527** (2010), 7832.
8) Z. Sami, S. Tahar and H. Mohamed: *Mater. Sci. Eng. A*, **598** (2014), 338.
9) N. Saeidi and A. Ekrami: *Mater. Sci. Eng. A*, **527** (2010), 5575.
10) H. Kawata and O. Umezawa: *ISIJ Int.*, **57** (2017), 1282.
11) T. Sirithanakorn, M. Tanaka and K. Higashida: *Mater. Sci. Eng. A*, **611** (2014), 383.
12) J. P. Naylor and P. R. Krahe: *Metall. Trans. A*, **6** (1975), 594.
13) G. R. Odette: *J. Nucl. Mater.*, **212**–**215** (1994), 45.
14) K. Edsinger, G. R. Odette, G. E. Lucas and J. W. Sheckherd: *J. Nucl. Mater.*, **233**–**237** (1996), 342.
15) K. W. Burns and F. B. Pickering: *J. Iron Steel Inst.*, **202** (1964), 899.
16) J. W. Morris, Jr.: *Mater. Res. Soc. Symp. Proc.*, **539** (1999), 23.
17) Y. Izumiyama, R. Kayano and R. Nagai: *Tetsu-to-Hagané*, **100** (2014), 704 (in Japanese).
18) L. Wang, D. Tang and Y. Song: *J. Iron Steel Res. Int.*, **24** (2017), 321.
19) O. Bouaziz and P. Buessler: *Adv. Eng. Mater.*, **6** (2004), 79.
20) H. Kawata and O. Umezawa: *Mater. Sci. Eng. A*, **716** (2018), 252.

© 2019 ISIJ